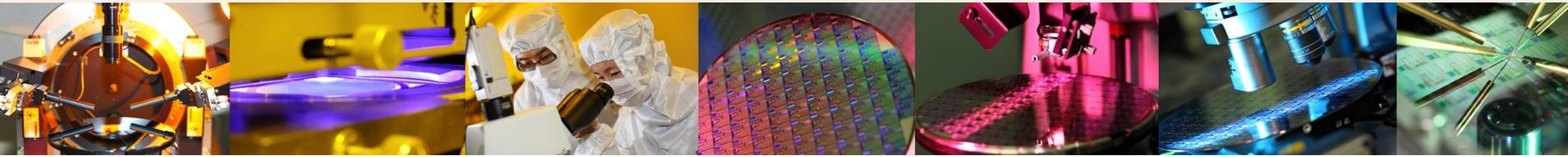
Development of 3D Sensors Based on CMOS Process

Work performed in the framework of the DRD3 WP2 project

"Novel silicon 3D-trench pixel detectors based on 8-inch CMOS process"

Manwen Liu, Huimin Ji, Peng Xu, Zhihua Li, Jun Luo (IMECAS, Beijing, China)
Xiaohui Li, Chenxi Fu, Xin Shi (IHEP, Beijing, China)
B. Hiti, G. Kramberger, B. Hiti, I. Mandić, A. Osterman, M. Puklavec, I. Velkovska (Jozef Stefan Institute, Ljubljana, Slovenia)
Zheng Li (Ludong University, Ludong, China)
M.v.Beuzekom , K. Akiba E. Chatzianagnosto (NIKHEF, Amstedam, Netherlands)
Gordana Medin (UCG-PMF, University of Montenegro, Podgorica, Montenegro)
Dengfeng Zhang (Central China Normal University, CCNU; University of Sheffield, Sheffield, UK)
G. Villani (STFC Rutherford Appleton Laboratory, UK)
Yanwen Liu, Kuo Ma (USTC, Hefei, China)
Suyu Xiao (SDIAT, Shandong Institute of Advanced Technology, Jinan, China)



INSTITUTE OF MICROELECTRONICS OF THE CHINESE ACADEMY OF SCIENCES
IMECAS
Univerzitet Crne Gore
中国科学技术大学 University of Science and Technology of China
湘潭大学 XIANGTAN UNIVERSITY
Nikhef 50
JSI Ljubljana Slovenia
University of Sheffield
Institute of High Energy Physics Chinese Academy of Sciences
CENTRAL CHINA NORMAL UNIVERSITY

Development of 3D Sensors Based on CMOS Process

Work performed in the framework of the DRD3 WP2 project

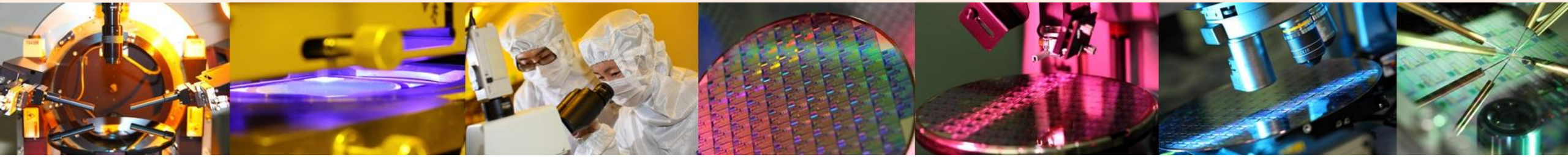
"Novel silicon 3D-trench pixel detectors based on 8-inch CMOS process"

6.1.2 Work Package – Sensors for 4D tracking

Project 2.1: Development of TI-LGADs for 4D Tracking
Project 2.2: US-Japan Development of Ultra-Fast-Time Low Mass Tracking Detectors
Project 2.3: Novel silicon 3-D trench pixel detectors on 8inch CMOS process
Project 2.4: Development of very small pitch ultra rad 3D sensors for 4D Tracking at FBK
Project 2.5: LGAD based timing tracker development for the future collider

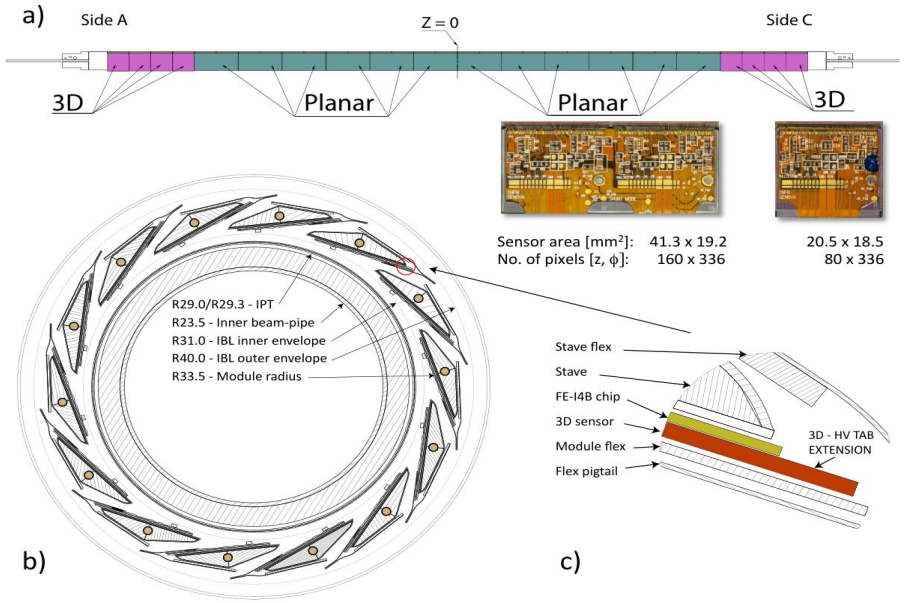
6.3.5.6 Responsible persons

Function	Name
Work Package Project Leader	Manwen Liu (IME-CAS)
Work Package Project Deputy Leader	Bojan Hiti

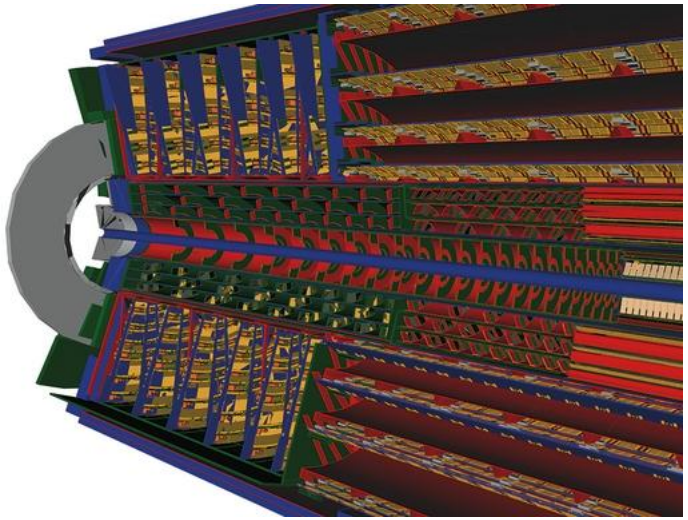


Background

- **The continuous upgrading and replacement of major scientific facilities have put forward higher requirements for the performance of sensors.**



Schematics of the IBL with the placement of the 3D modules at the ends of the staves: (a) Stave layout with the organization of planar and 3D sensor modules. (b) Layout of the IBL detector with the 14 staves around the IBL positioning tube (IPT) and (c) zoom of one stave side where a 3D sensor module is visibile. ©2015 IOP Publishing Ltd and Sissa Medialab srl. All rights reserved. https://doi.org/10.1088/1748-0221/10/05/C05001

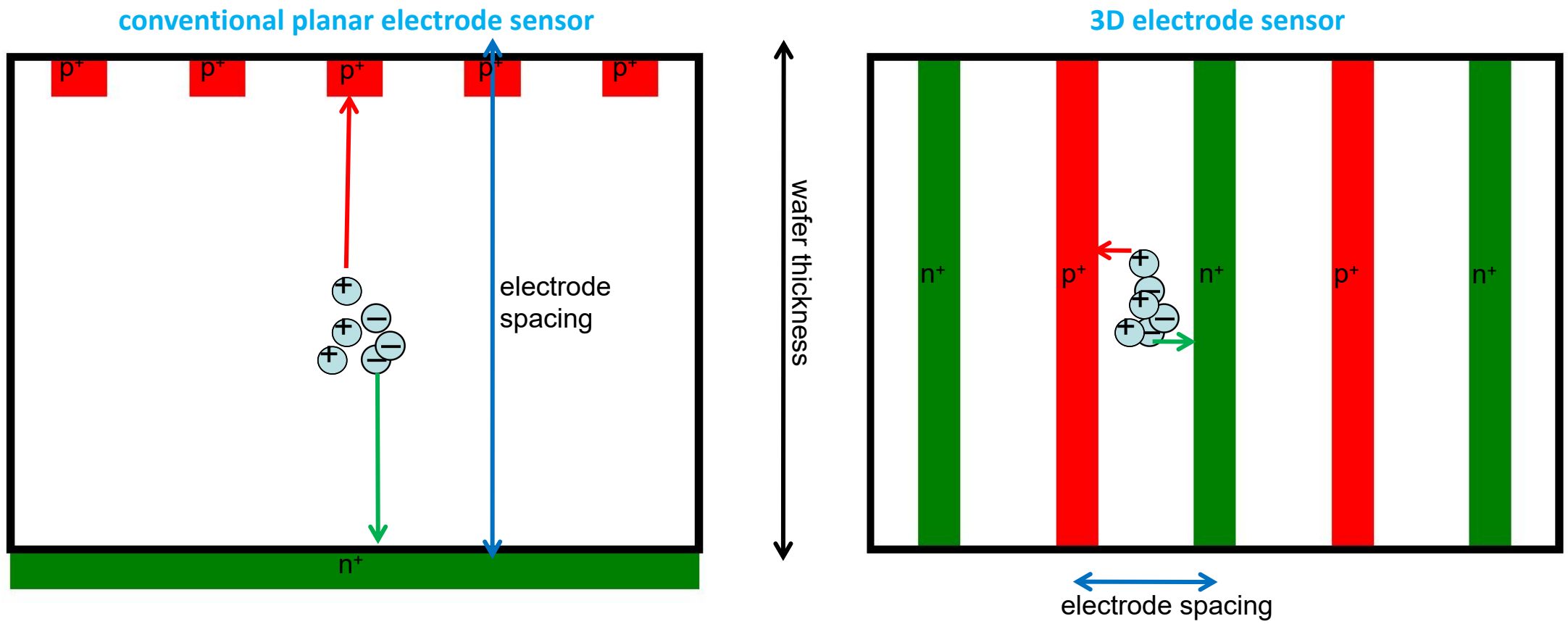


The ATLAS ITk, comprising strip (outer layers) and pixel (inner layers) detectors with more than five billion readout channels. (Image: ATLAS Collaboration/CERN)

- The Large Hadron Collider (LHC) and Future Circular Collider (FCC) at CERN
- Beijing Electron-positron Collider, Shanghai Synchrotron Radiation Facility
- Large Circular Electron-Positron Collider (CEPC), X-ray free Electron Laser

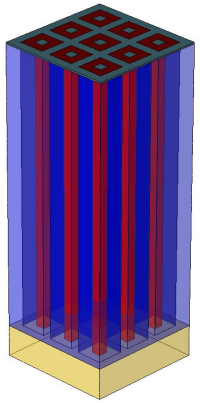
3D Sensors

- **Compared with planar sensors, 3D detectors have the following advantages: fast response, radiation hardness, low power consumption and low noise.**

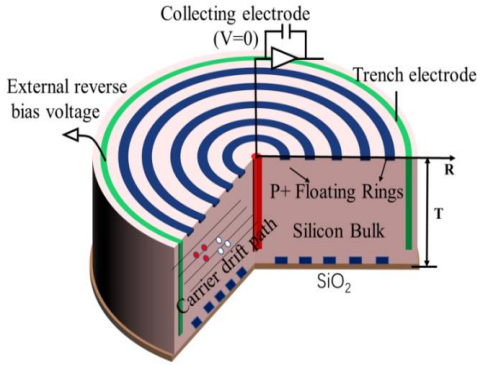


3D Sensors

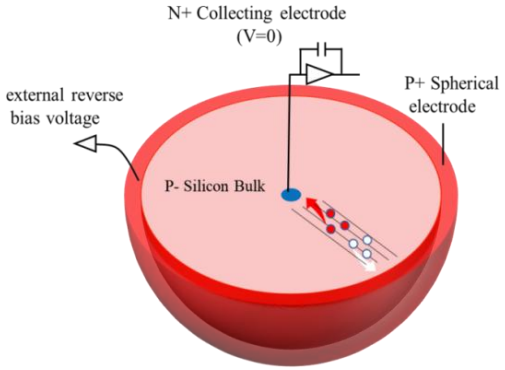
- **In the early stage, multiple theoretical models of 3D trench electrode sensors were proposed and verified through TCAD simulation.**



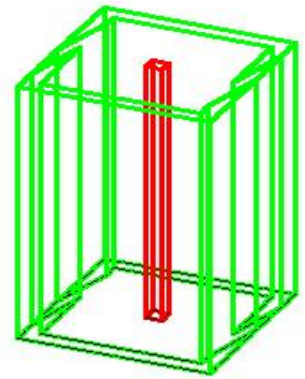
Ultra-fast, radiation-resistant

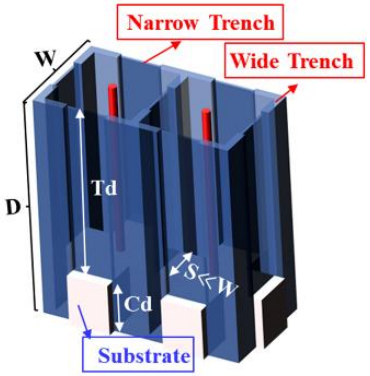


Large area, small proportion of dead zones

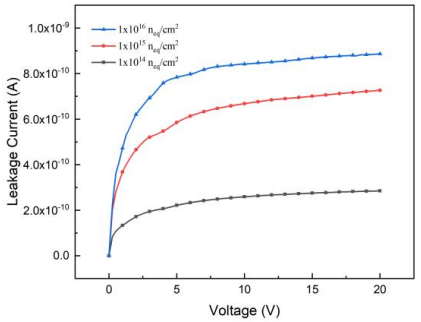


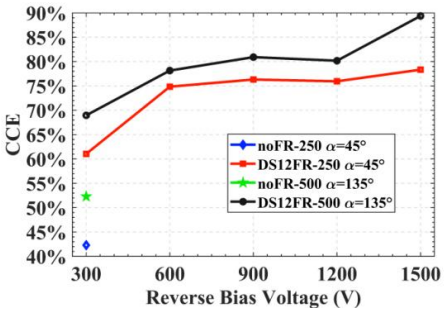
Low capacitance, uniform electric field distribution

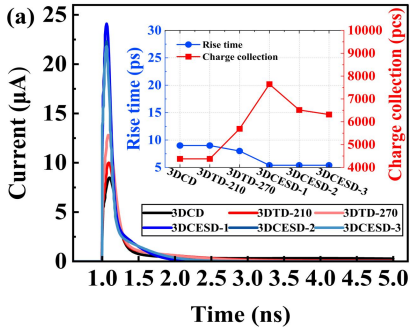




small proportion of dead zones, Through-etching







TCAD simulation verified its strong radiation resistance, high charge collection, and ultrafast time characteristics

3D Sensors with Gain

What about silicon 3D detectors – can they have gain?

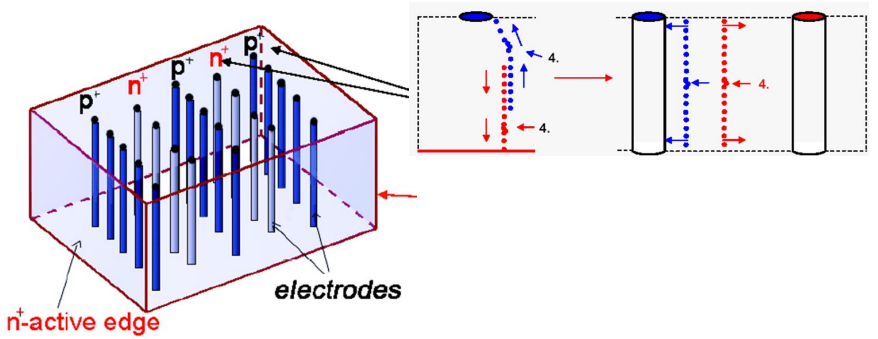
- The doping of columns of 3D detectors is almost impossible to control with the required precision – achieving high enough **electric field with doping is not possible (no LGAD like solution)**

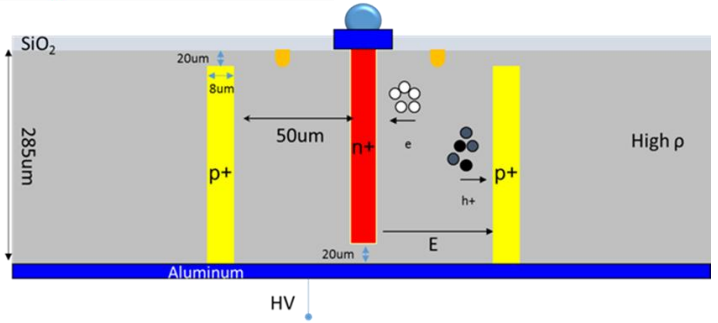
- The aspect ratio of HEP producers (FBK, CNM, Sintef) have been 25:1 so thick detector had column widths of ~10 μm which also limited cell sizes to ~50x50 μm² (25x100 μm²) – current ATLAS/CMS pixels.

- We have observed gain multiplication in irradiated devices in the past (ATLAS/CMS) at the tips of the electrodes – which actually limits the operation voltage for those detectors.

- During the ECFA detector R&D roadmap document preparation: **"Improvements of aspect ratio to 100:1 would lead to manufacturing of very narrow columns <1 μm with thicknesses of ~100 μm which could lead to electric fields high enough (~30 V/μm) for multiplication"**

- The CMOS processing line at **IME-CAS Beijing** has properties which are required for achieving the gain through geometry.







3D Sensors with Gain

➢ IMECAS 3D Column-Trench silicon sensor with internal gain

IME 8” CMOS process

- 30-35 μm thick epi on thick substrate
- **n⁺** columns on **p type** bulk
- $N_{eff}=2\cdot10^{13}$ cm^{-3}
- **ASPECT RATIO OF 70:1**

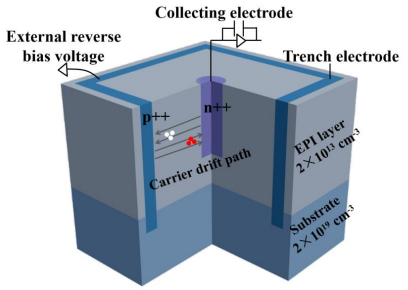
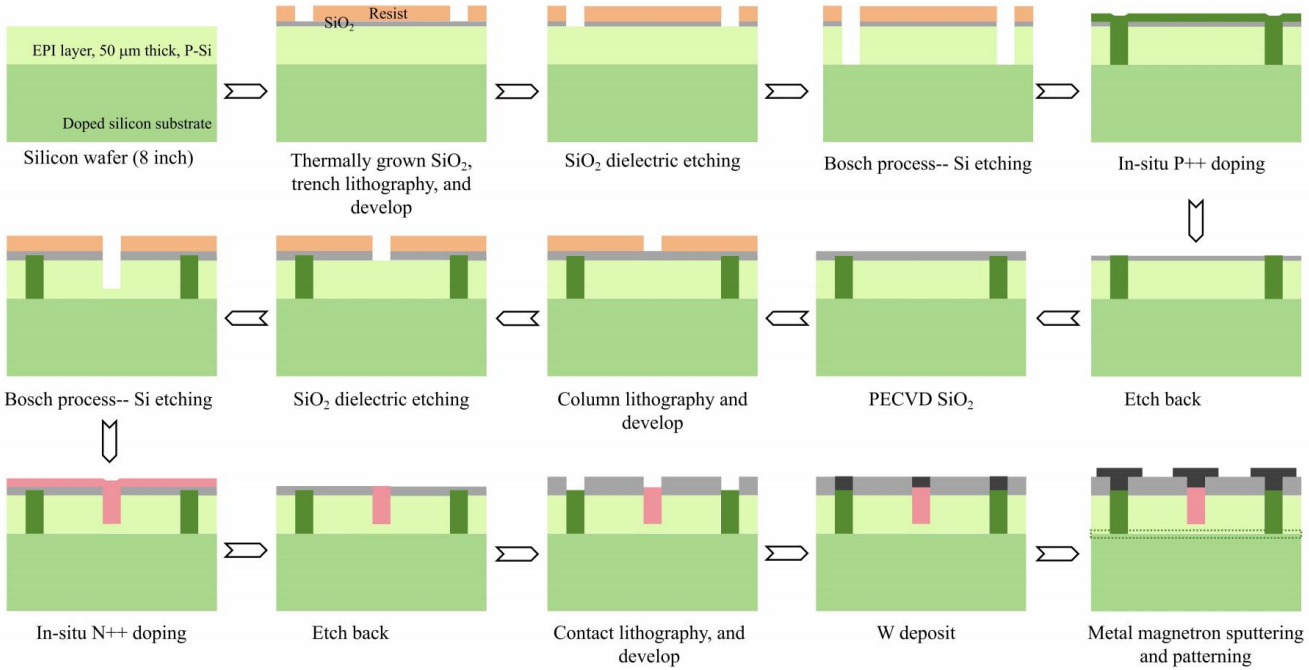
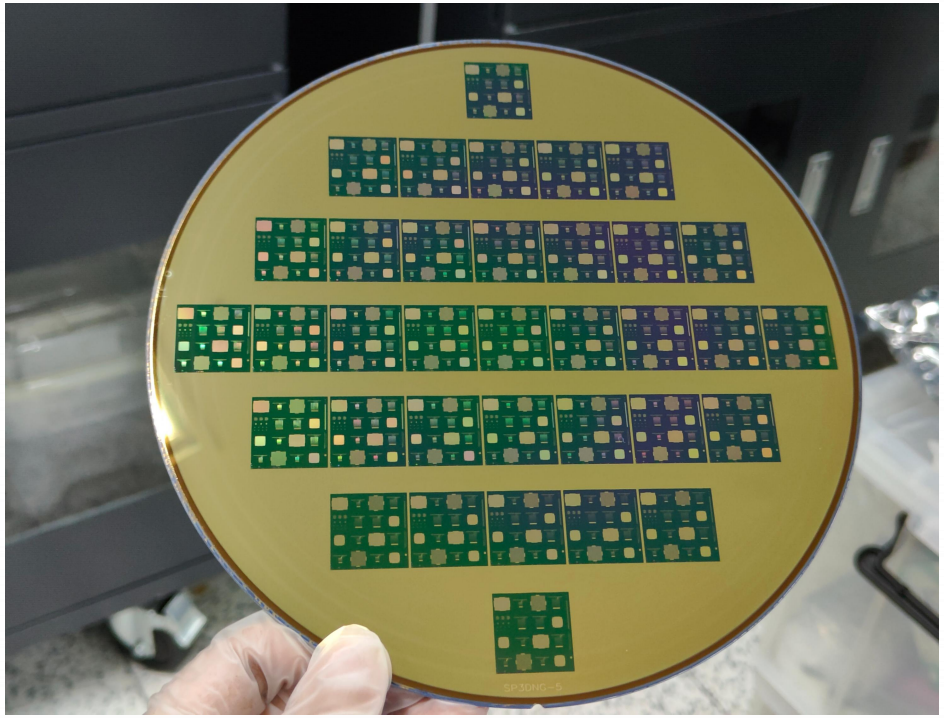


Fig. 1: The schematic of the 3D Trench-Column Sensor.

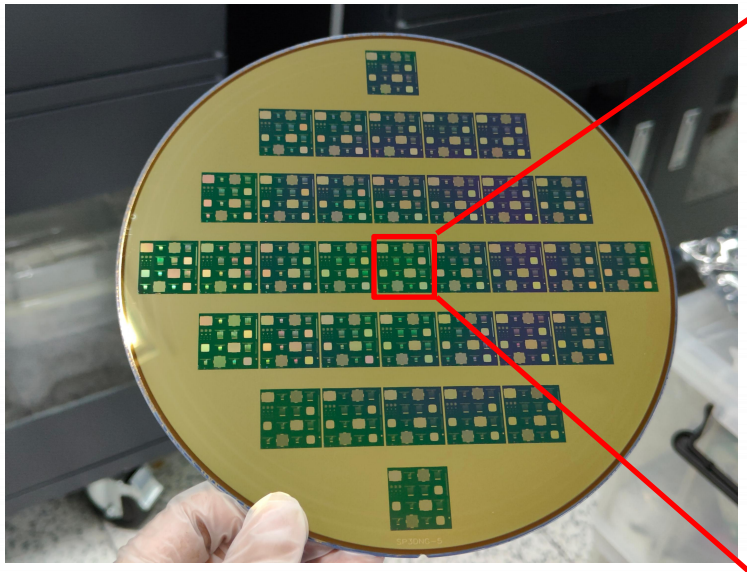


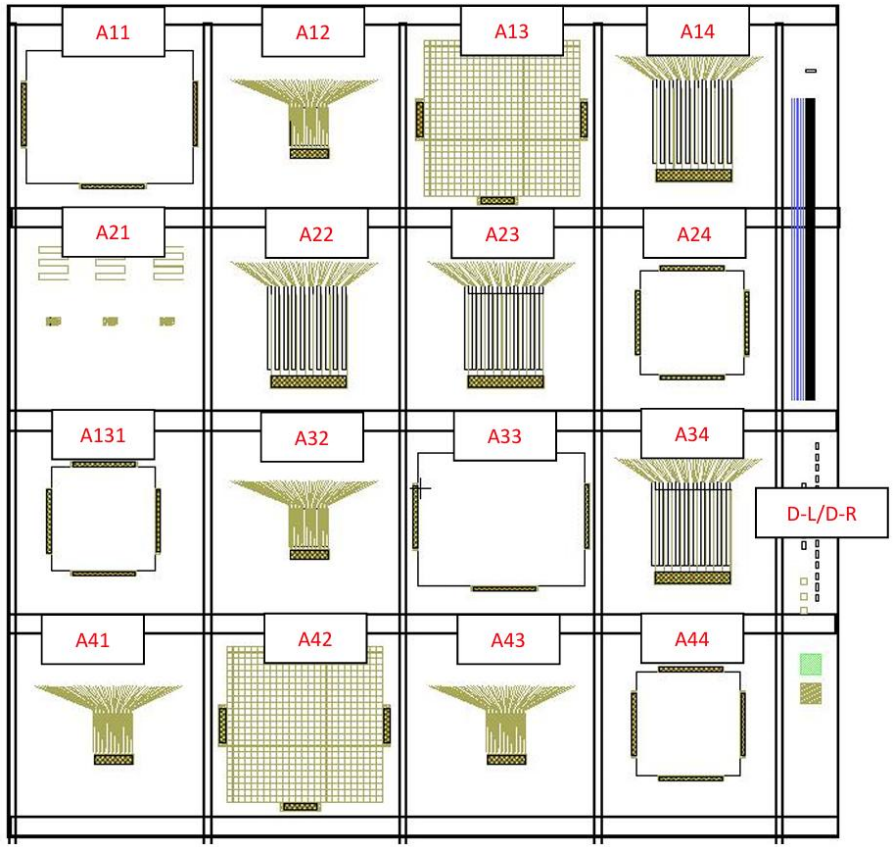


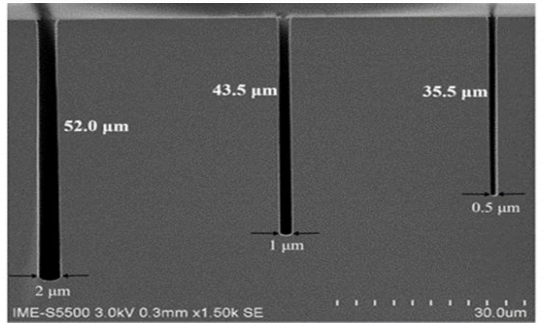
M. Liu et al., IEEE Trans. Nucl. Sci., vol. 73, no. 1, Jan. 2026.

3D Sensors with Gain

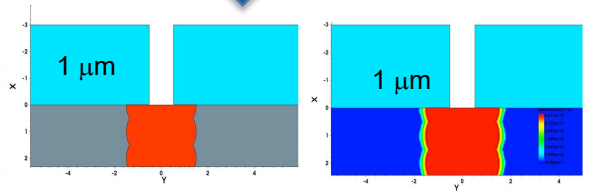
➢ IMECAS 3D Column-Trench silicon sensor with internal gain



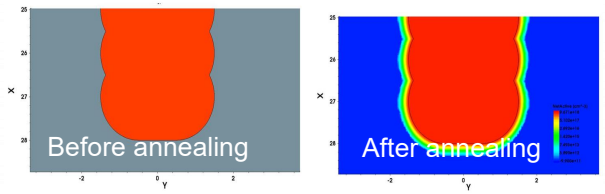




SIMULATION OF THE DOPING



After column doping effective width increases



IME 8" CMOS process

- 30-35 µm thick epi on thick substrate
- **n⁺** columns on **p type** bulk
- $N_{eff}=2\cdot10^{13}$ cm^{-3}
- **ASPECT RATIO OF 70:1**

M. Liu et al., IEEE Trans. Nucl. Sci., vol. 73, no. 1, Jan. 2026.

3D Sensors with Gain

- **Simulation and measurement results in IMECAS, RAL(Rutherford Appleton Laboratory) and University of Sheffield**

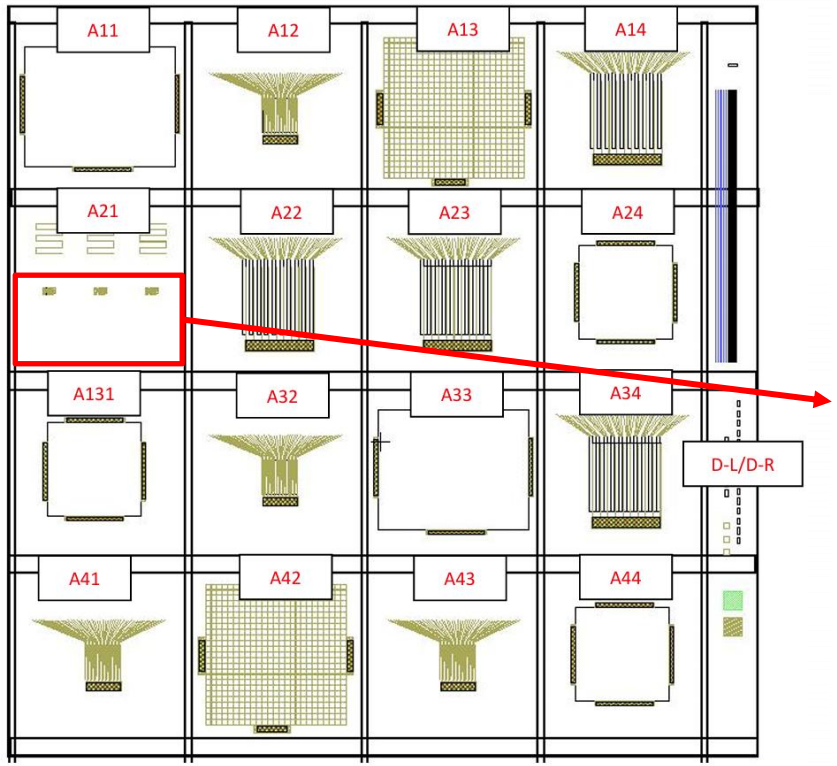
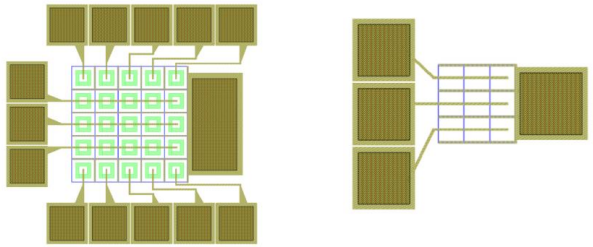


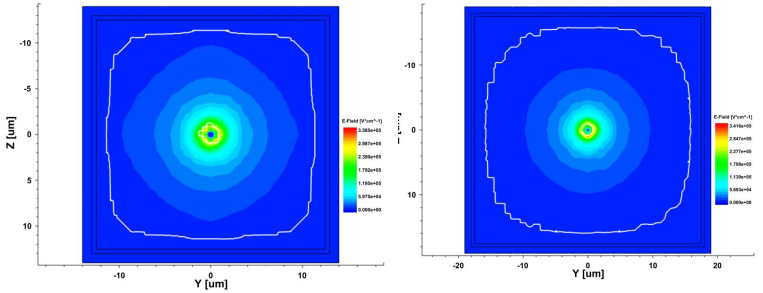
TABLE I: Layouts of 3D Trench-Column pixel devices: A21-21 and A21-43.

Layout	Trench Shape	Electrode Width [μm]	Array	Pixel Size [μm]
A21-21	Square	0.5	5×5	35×35
A21-43	Square	0.5	3×3	25×25

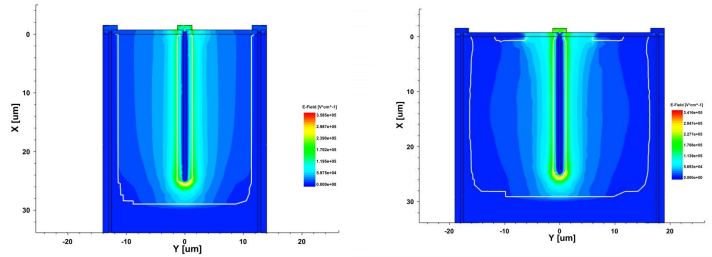


(a) (b)

Fig. 2: Layouts of the 3D Trench-Column pixel array, (a) A21-21: 5×5 pixel array with the pixel size of 35×35 μm, (b) A21-43: 3×3 pixel array with the pixel size of 25×25 μm. The pad on the right is connected to the trench electrode which is conductive to the substrate, the other pads are connected to the central cathode electrodes.



Cutaway view of the simulated electric field in the *YZ* plane at thedepth of 25 μm of (a) A21 – 43 and (b) A21 – 21 at the reverse bias voltageof 50 V.

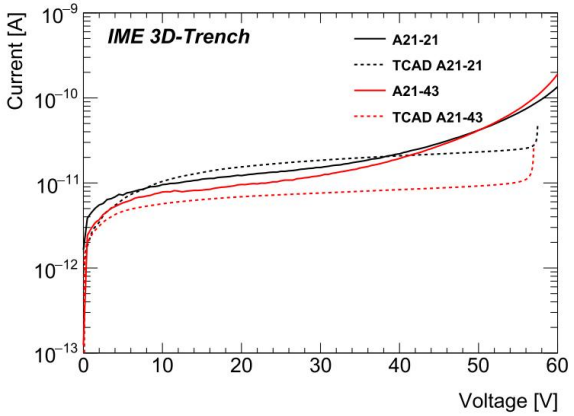


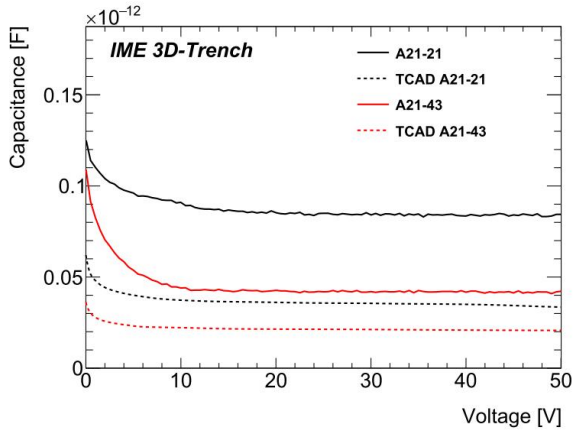
Cutaway view of the simulated electric field in the *XY* plane crossingthe *z*-axis of (a) A21 – 43 and (b) A21 – 21 at the reverse bias voltage of 50 V.

M. Liu et al., IEEE Trans. Nucl. Sci., vol. 73, no. 1, Jan. 2026.

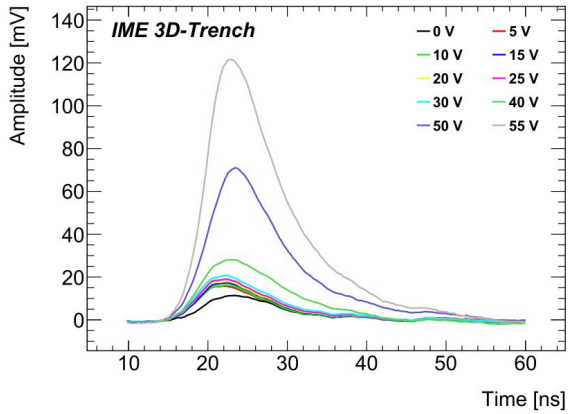
3D Sensors with Gain

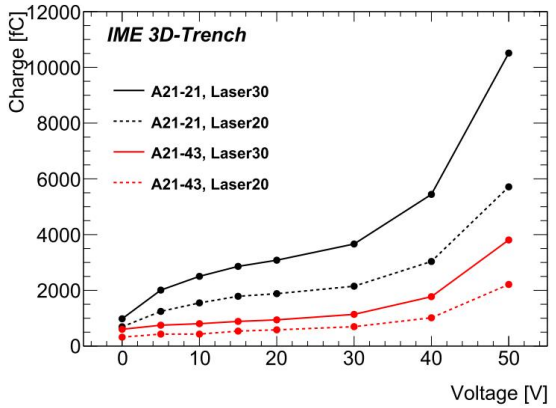
➢ Simulation and measurement results in IMECAS, RAL and University of Sheffield

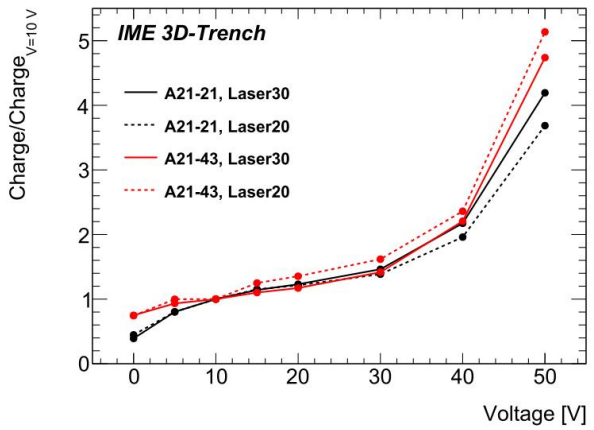








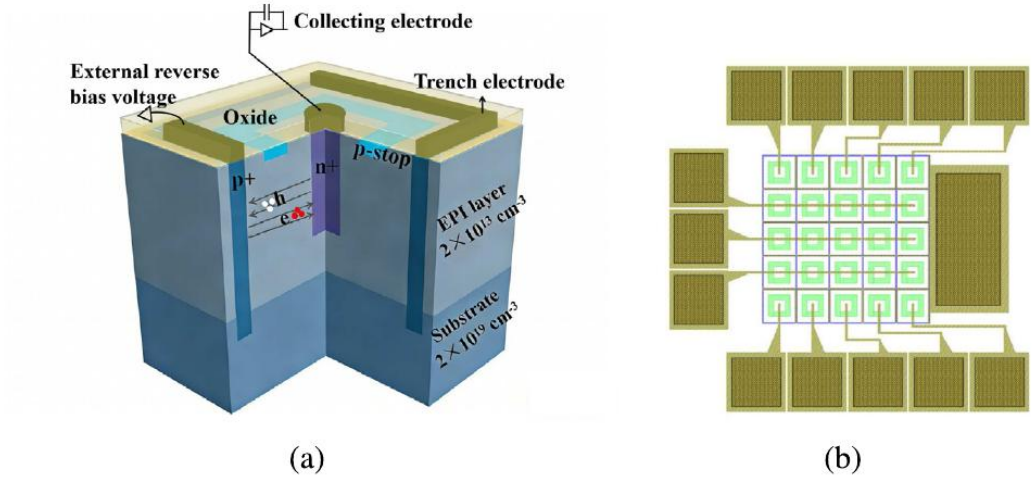




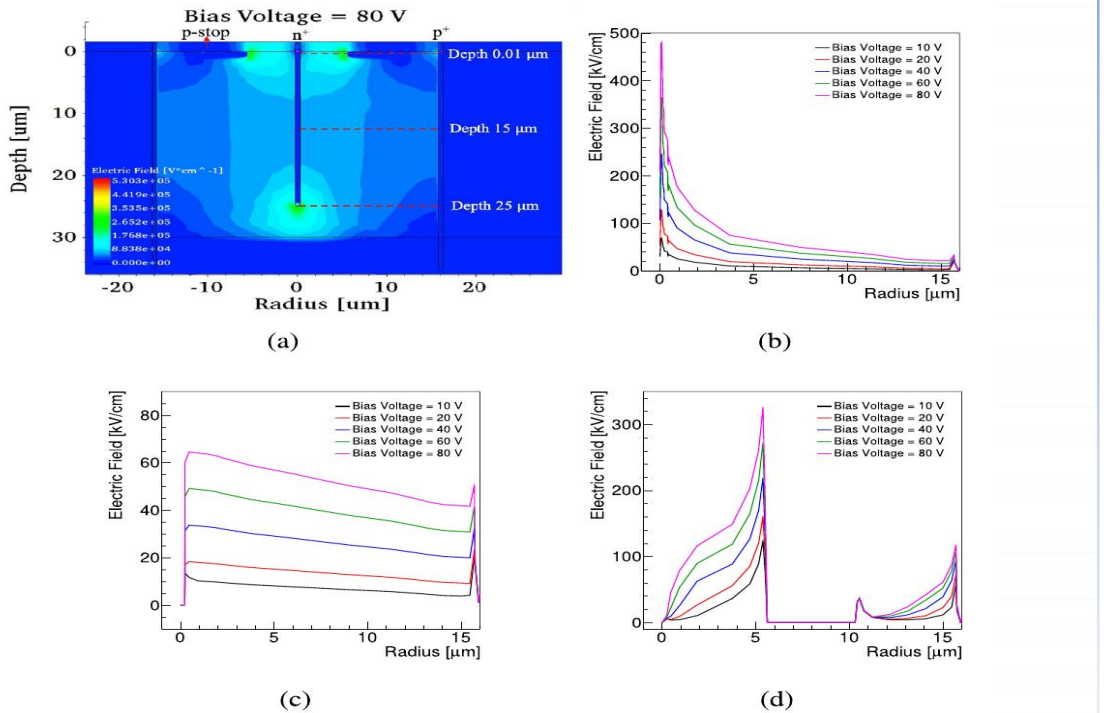
M. Liu et al., IEEE Trans. Nucl. Sci., vol. 73, no. 1, Jan. 2026.

3D Sensors with Gain

➢ Trench-column geometry and avalanche mechanism



Sensor geometry and 5 × 5 array with 35 × 35 μm² pixels.



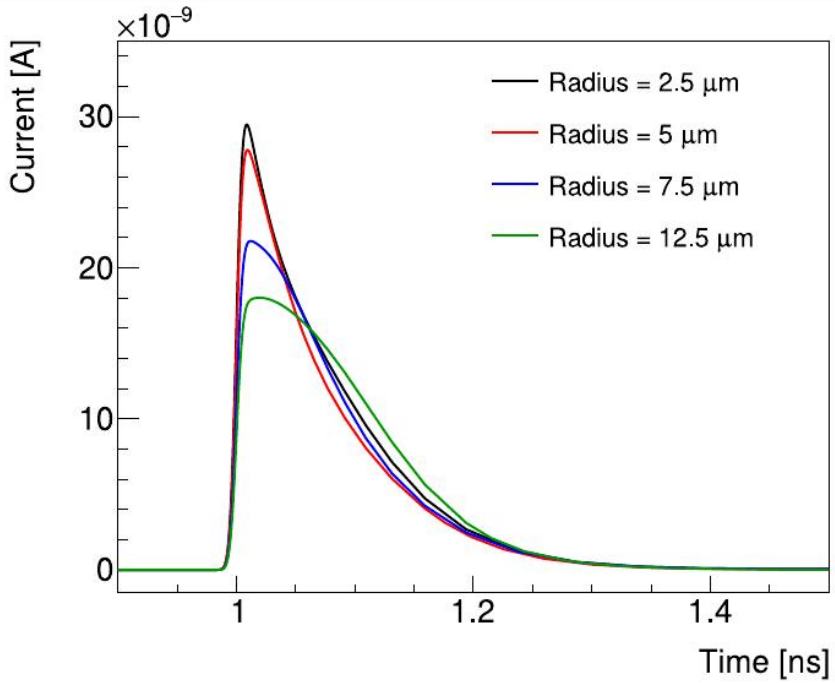
Electric field at 80 V and radial profiles at selected depths.

A submicron collection column creates a high electric field for intrinsic charge multiplication.

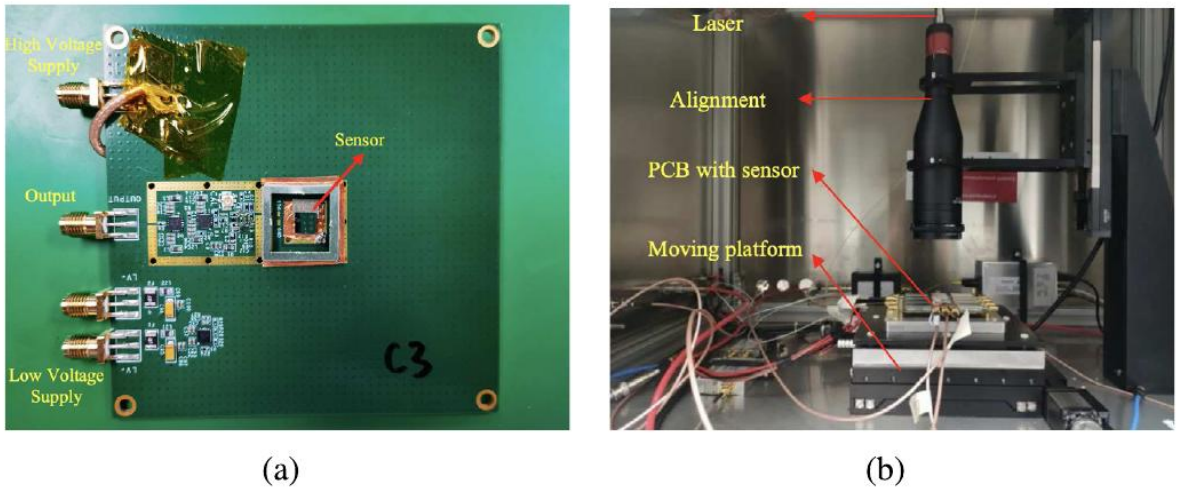
M. Liu et al., NIM A 1093 (2027) 172084, doi:10.1016/j.nima.2026.172084.

3D Sensors with Gain

➢ Simulation and experimental setup



Simulated transient currents at different laser injection radii, 80 V.



(a) (b)

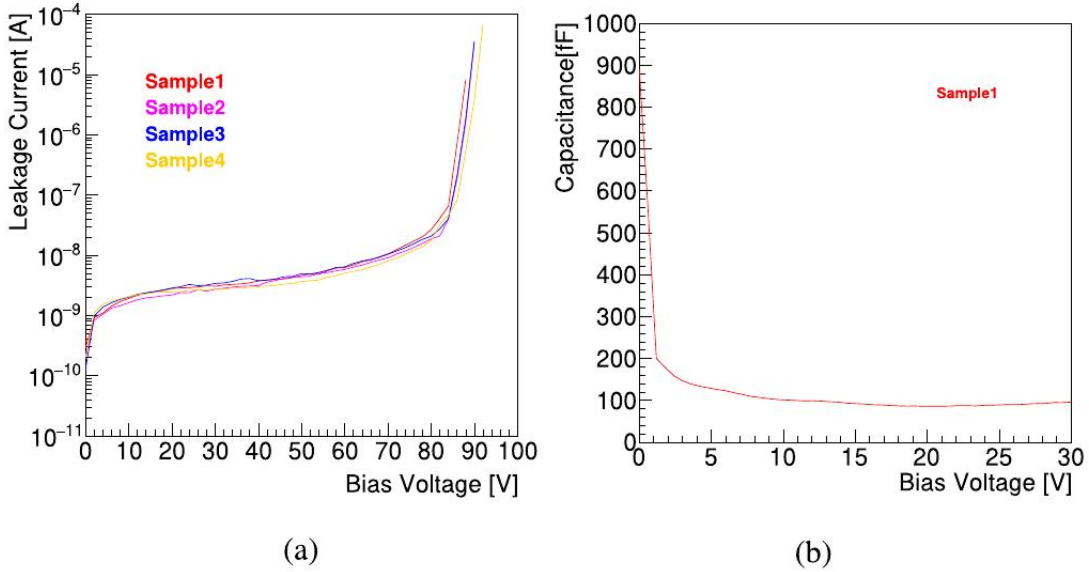
Sensor on the amplifier board and infrared TCT setup.

TCAD predicts fast charge collection, while the readout bandwidth limits measured pulse shapes.

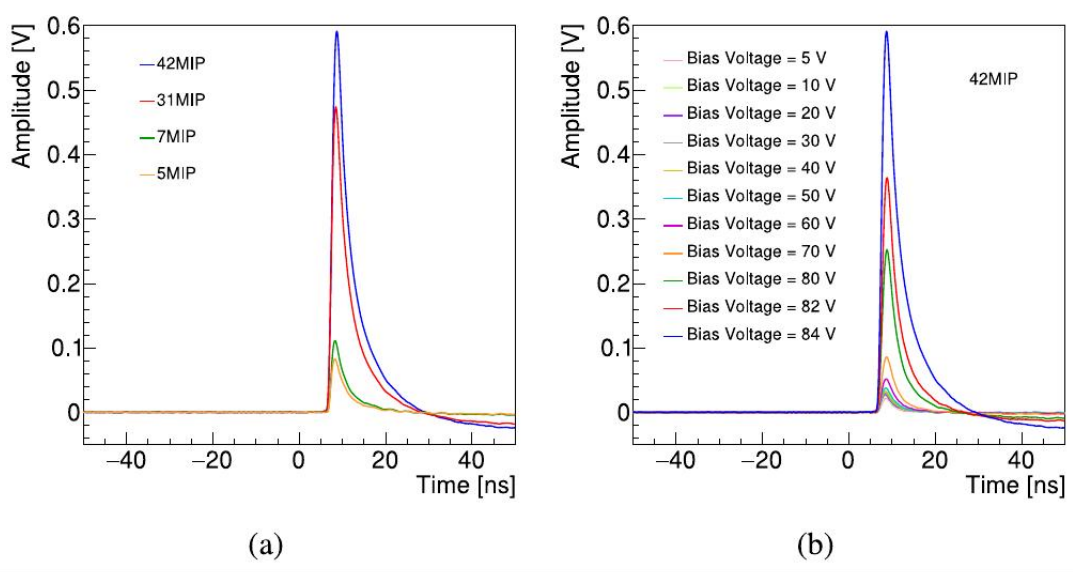
M. Liu et al., NIM A 1093 (2027) 172084, doi:10.1016/j.nima.2026.172084.

3D Sensors with Gain

➢ Electrical characteristics and laser waveforms



Measured leakage current and capacitance versus reverse bias.



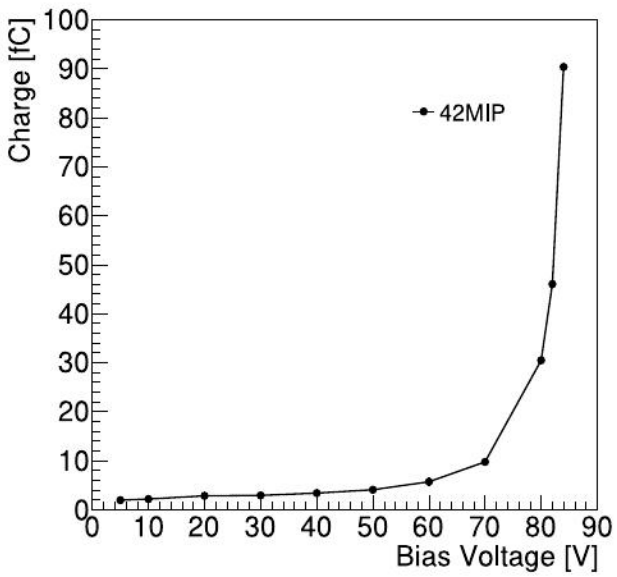
Averaged TCT waveforms versus laser intensity and bias voltage.

The sensor shows low leakage below breakdown and increasing signal amplitude at high bias.

M. Liu et al., NIM A 1093 (2027) 172084, doi:10.1016/j.nima.2026.172084.

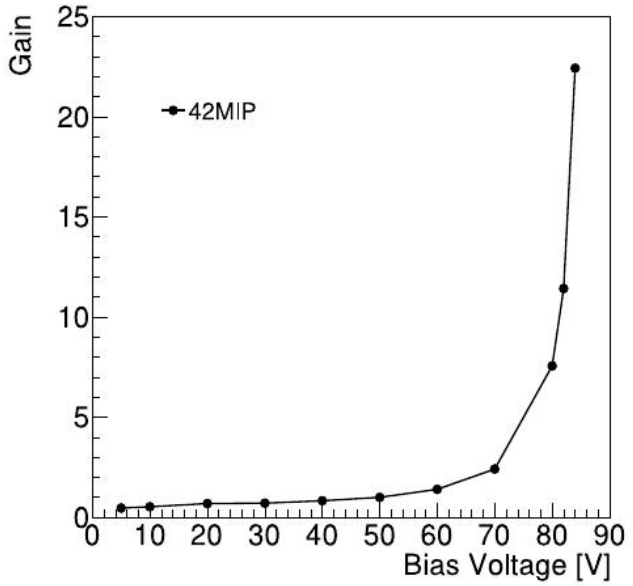
3D Sensors with Gain

➢ Laser charge multiplication and timing



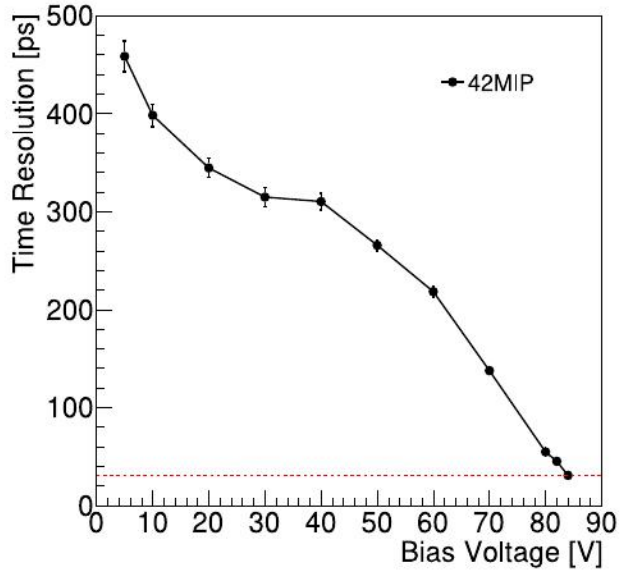
(b)

Collected charge versus bias voltage.



(c)

Laser gain versus bias voltage.



(e)

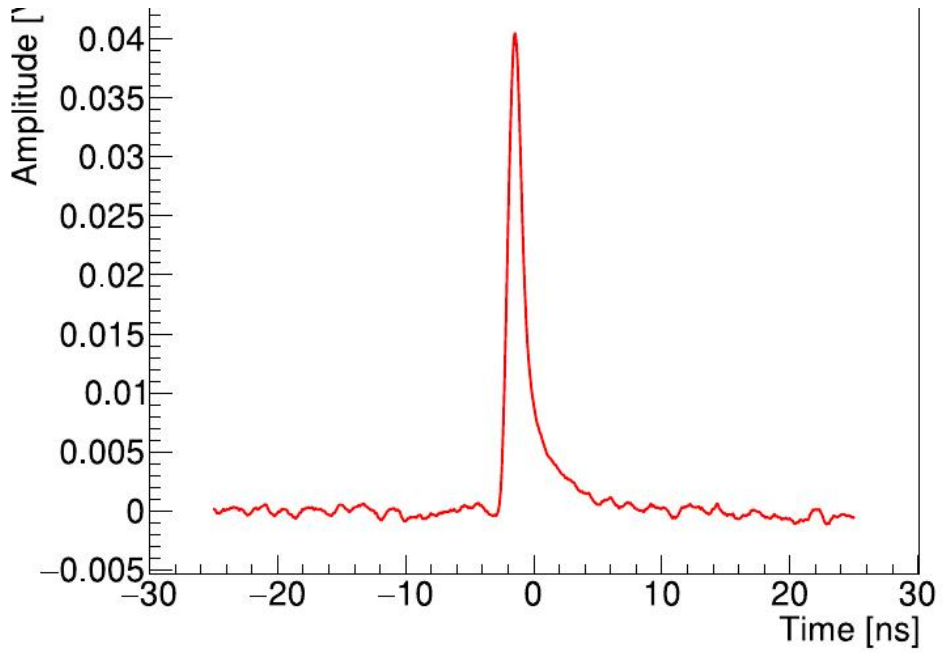
Fixed-position laser timing versus bias.

At 84 V, fixed-position 42-MIP laser injection yields gain ≈22.42 and timing of 30.72 ± 0.71 ps.

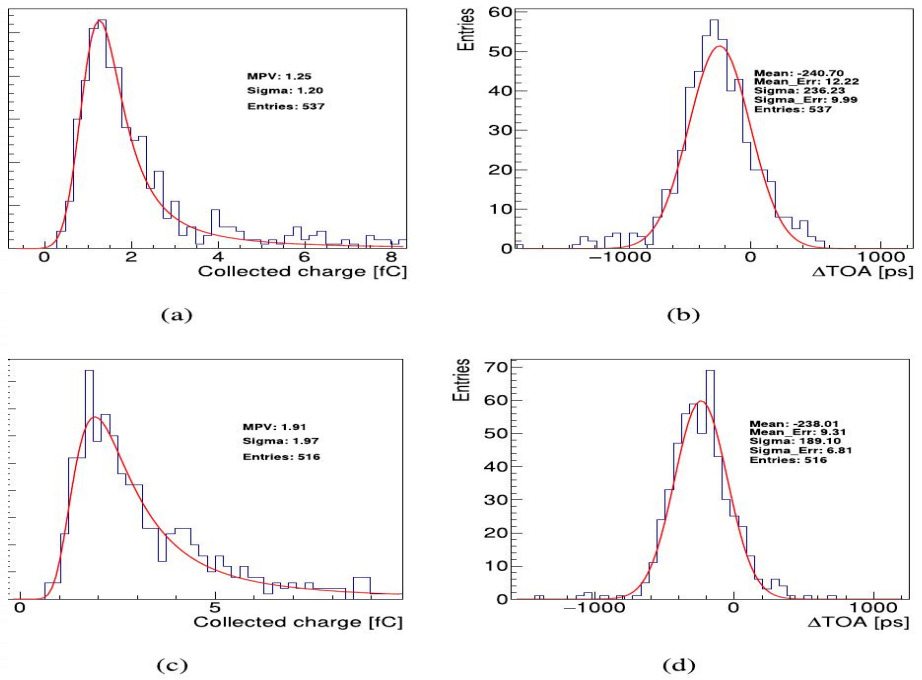
M. Liu et al., NIM A 1093 (2027) 172084, doi:10.1016/j.nima.2026.172084.

3D Sensors with Gain

➢ Beta-source validation and temperature dependence



Average beta-source waveform at 84 V and 20 °C.



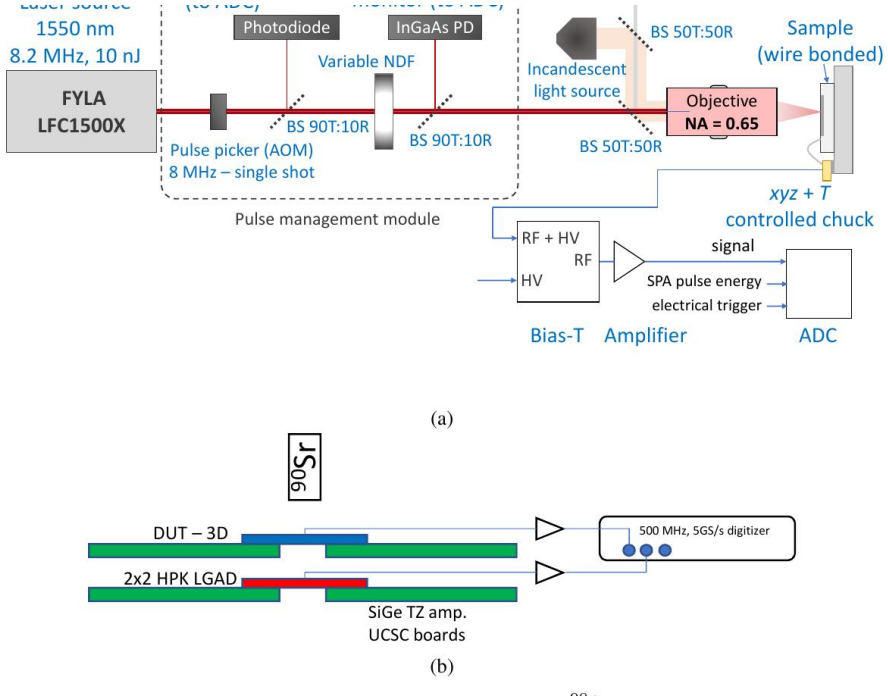
Charge and ΔTOA distributions at 20 °C and −30 °C, 84 V.

At 84 V, cooling from 20 °C to −30 °C raises beta-source gain from 4.17 to 6.37 and improves timing from 232 to 182 ps.

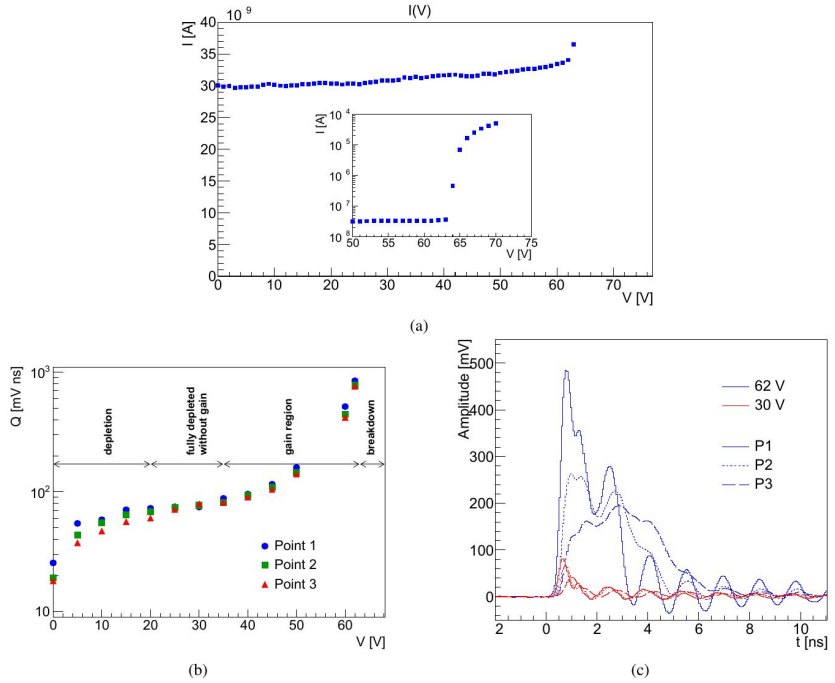
M. Liu et al., NIM A 1093 (2027) 172084, doi:10.1016/j.nima.2026.172084.

3D Sensors with Gain

➢ TPA-TCT and beta-source measurement methods



TPA-TCT optical chain and ^{90}Sr timing measurement setup.



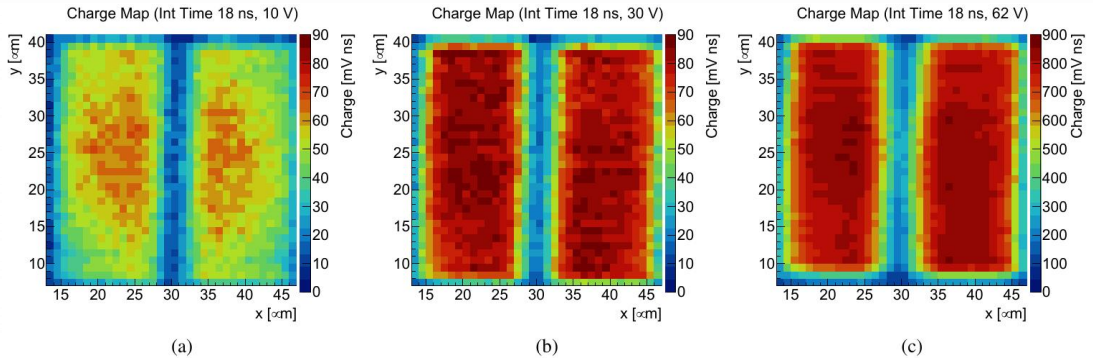
I–V, collected charge versus bias and representative waveforms.

TPA-TCT resolves local gain, and beta-source measurements independently test particle response.

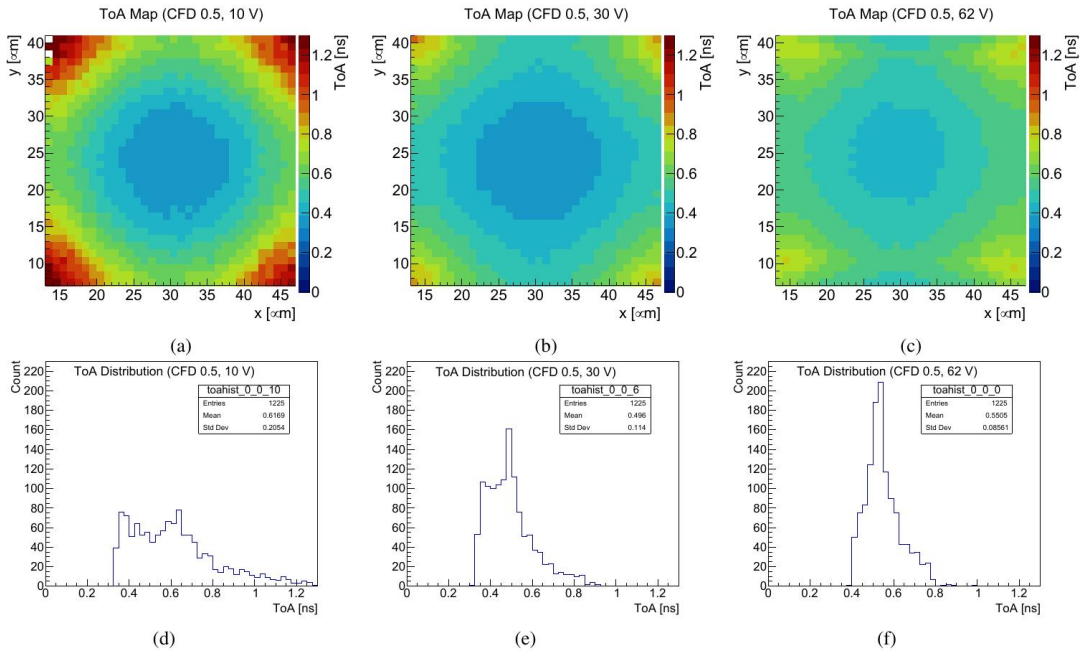
B. Hiti, Manwen Liu* et al., Small cell 3D detectors with intrinsic gain, IEEE TNS, doi:10.1109/TNS.2026.3738892.

3D Sensors with Gain

➢ Spatial uniformity of charge collection and timing



Charge maps across the cell at 10, 30 and 60 V.



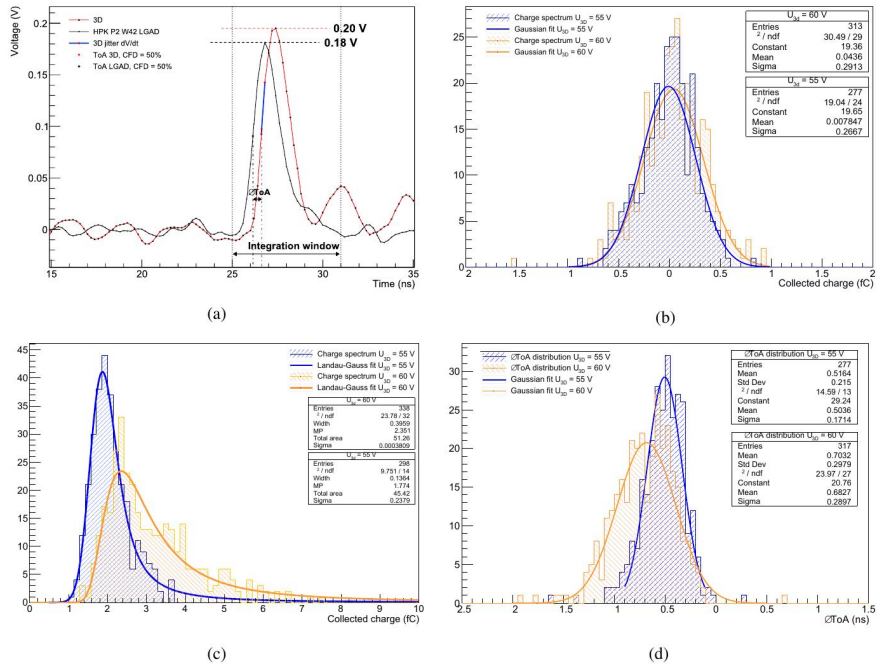
ToA maps and distributions at 10, 30 and 60 V, CFD = 0.5.

Higher bias improves charge collection, but the central column and trench corners retain position-dependent timing.

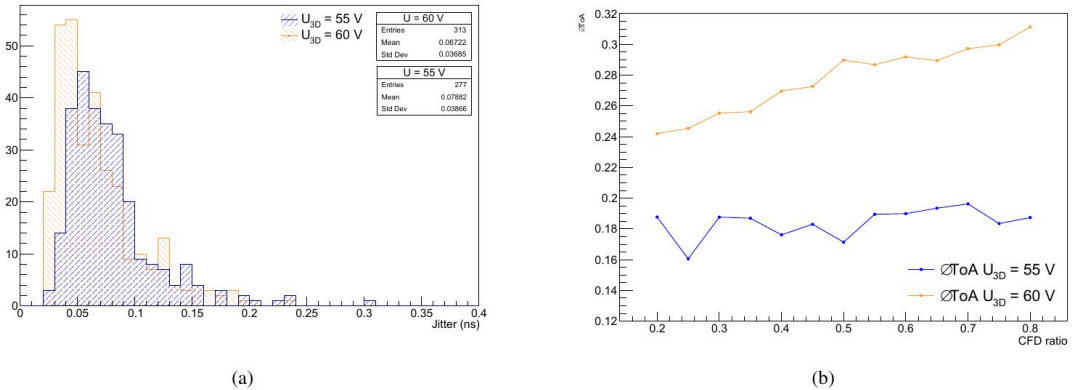
B. Hiti, Manwen Liu* et al., Small cell 3D detectors with intrinsic gain, IEEE TNS, doi:10.1109/TNS.2026.3738892.

3D Sensors with Gain

➢ Particle timing and stable intrinsic gain



Beta-source waveforms, charge and timing distributions at 55 and 60 V.



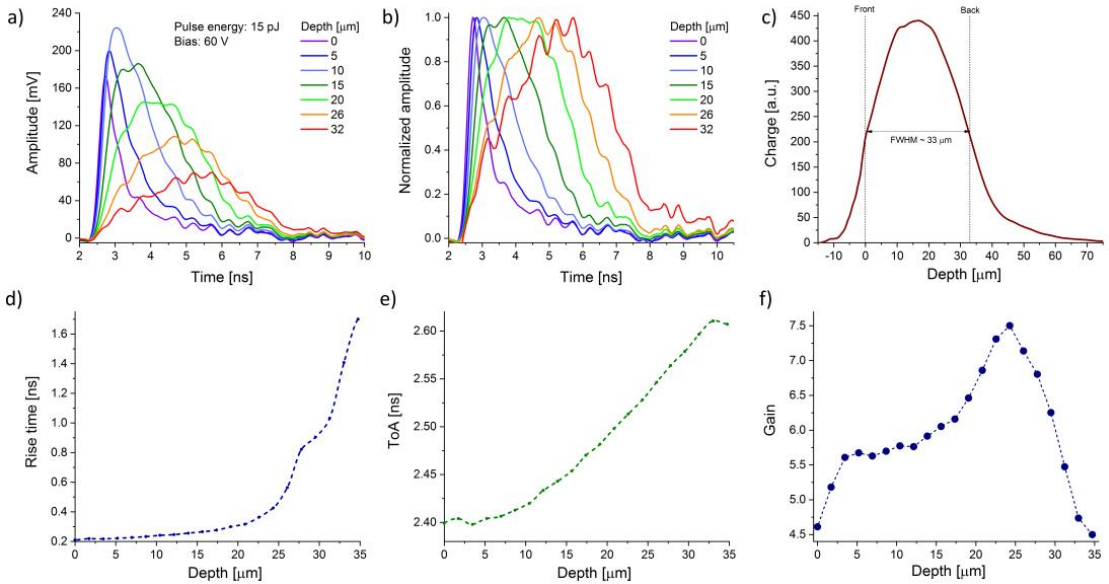
Noise jitter and time resolution versus CFD fraction.

Stable gain reaches about 8, while beta-source timing is ≈160 ps at 55 V and ≈280 ps at 60 V.

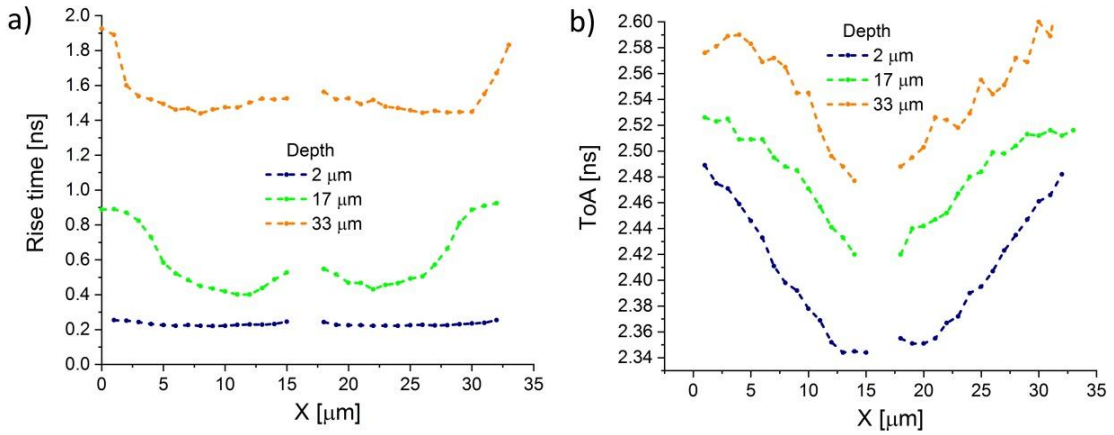
B. Hiti, Manwen Liu* et al., Small cell 3D detectors with intrinsic gain, IEEE TNS, doi:10.1109/TNS.2026.3738892.

3D Sensors with Gain

➢ Depth-resolved charge transport



Waveforms, charge, rise time, ToA and gain versus injection depth.



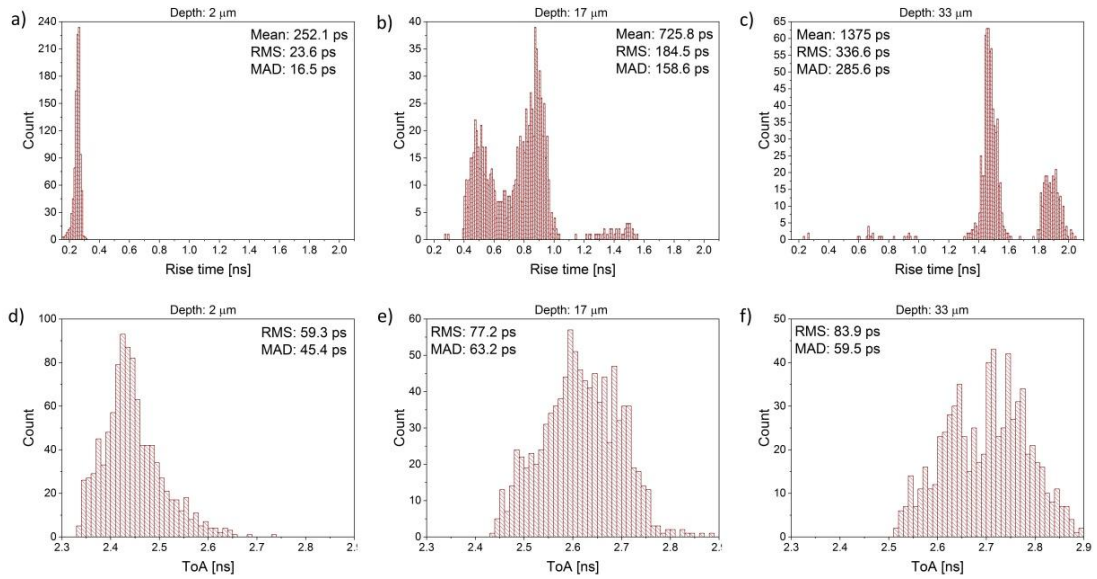
Lateral rise-time and ToA profiles at depths of 2, 17 and 33 µm.

Depth scans reveal slower carrier transport near the substrate and weaker-field trench regions.

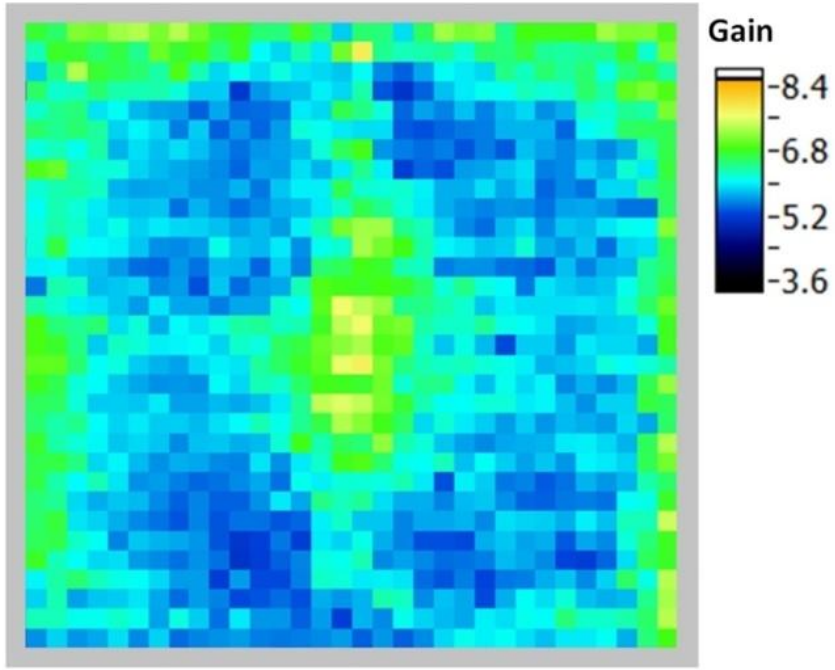
G. Lastovicka-Medin, M. Liu et al., Thin 3D Trench Silicon Detectors with Submicron Electrodes, JINST, 2026.

3D Sensors with Gain

➢ Gain uniformity and timing dispersion



Rise-time and ToA distributions at 2, 17 and 33 μm depth.



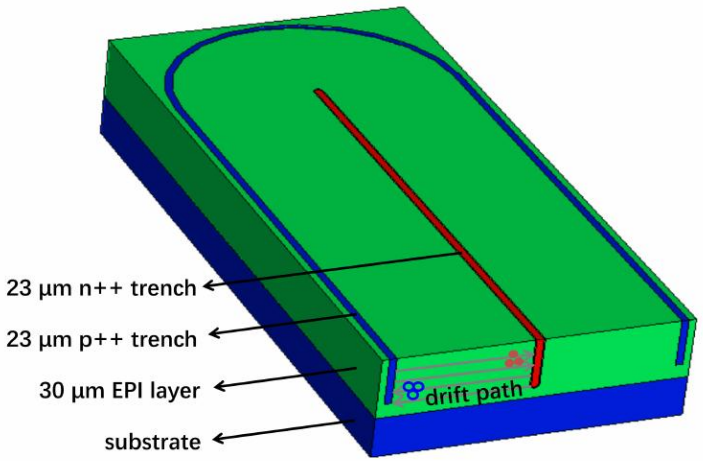
Gain map at 60 V, 15 pJ and 17 μm depth.

Gain varies laterally by about 20–25%, and the spatial ToA RMS rises from 59.3 to 83.9 ps with depth.

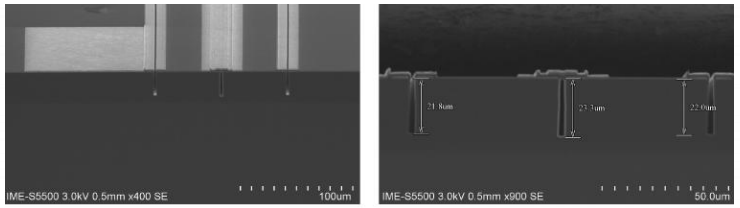
G. Lastovicka-Medin, M. Liu et al., Thin 3D Trench Silicon Detectors with Submicron Electrodes, JINST, 2026.

Racetrack 3D Sensors

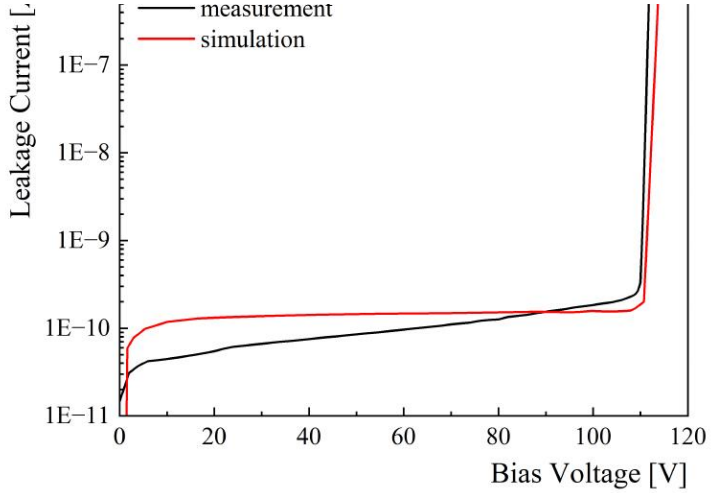
➢ Racetrack geometry and electrical performance



Half view of the racetrack sensor with a long collection electrode.



Surface and cross-sectional SEM images.



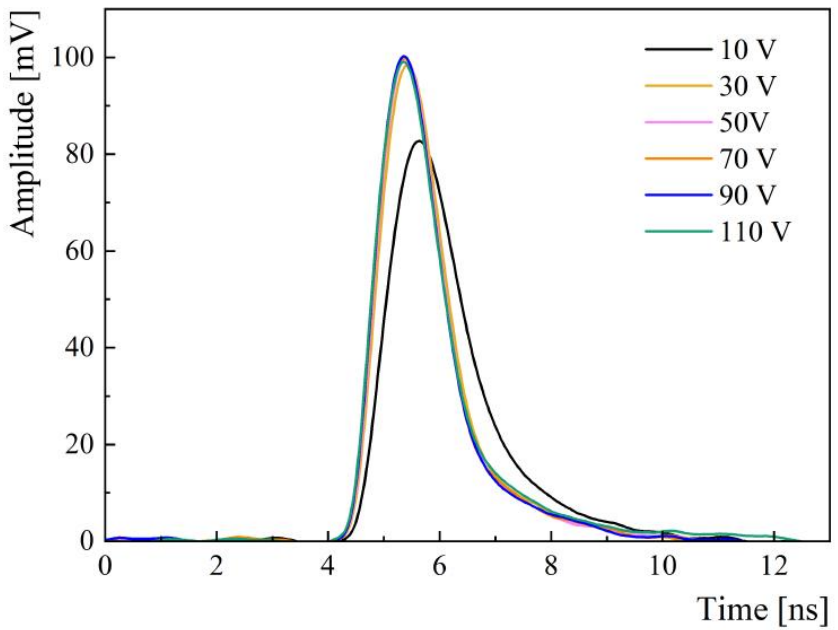
Measured and simulated I–V characteristics.

The 23-μm-deep racetrack structure achieves leakage below 0.16 nA at 90 V and breakdown above 110 V.

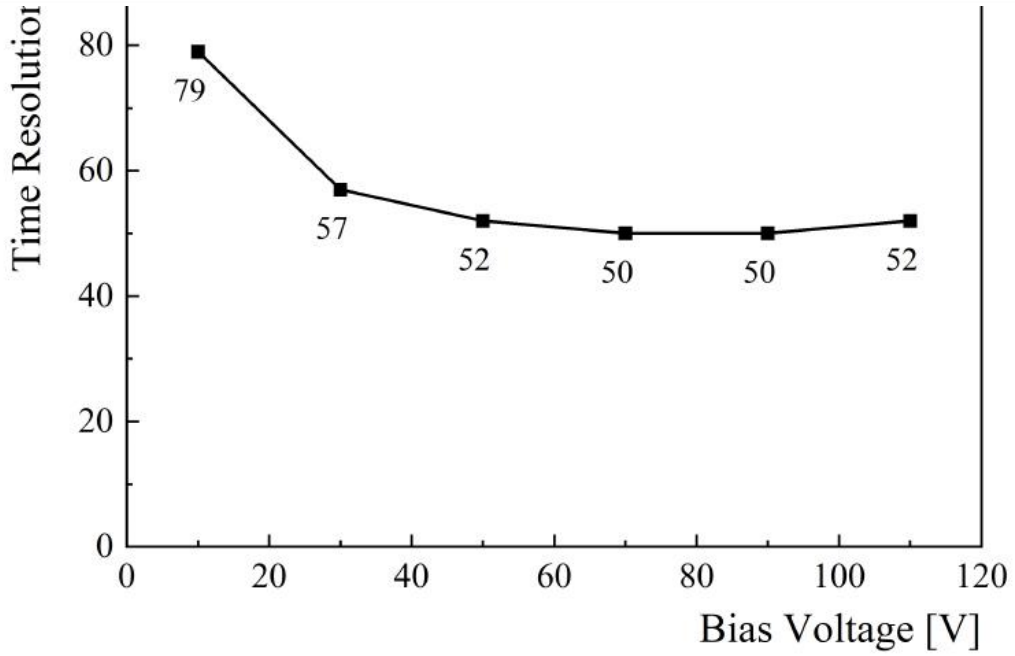
H. Ji, M. Liu* et al., Design and Characterization of Racetrack 3D-Trench Silicon Sensor Based on 8-Inch Process, supplied manuscript.

Racetrack 3D Sensors

➢ Racetrack laser response and timing



Average waveforms under fixed-position 11-MIP-equivalent laser injection.



Width of the ΔTOA distribution versus bias voltage.

At 90 V, fixed-position 11-MIP laser injection gives about 4 fC, a 634 ps rise time and σ(ΔTOA) ≈50 ps.

H. Ji, M. Liu* et al., Design and Characterization of Racetrack 3D-Trench Silicon Sensor Based on 8-Inch Process, supplied manuscript.

Conclusion

1. The IMECAS 8-inch CMOS process enables 30-μm-thick trench-column sensors with 0.5-μm columns and intrinsic gain without a dedicated gain layer.

2. Laser and beta-source measurements confirm charge multiplication. In the NIM A study, fixed-position laser timing reaches about 31 ps, while beta-source timing reaches about 182 ps at −30 °C and 84 V.

3. TPA-TCT identifies gain and timing variations across the cell and through its depth. Electric-field uniformity and readout bandwidth remain key targets for improvement.

4. Racetrack sensors demonstrate about 50 ps laser ΔTOA spread at a fixed position. The simulated X-ray sensor concepts extend the platform toward X-ray detection and require further experimental validation.

Thank you!

